Supporting Information

Accelerated Exciton Dissociation and Electron Extraction across Metallic Sulfide-Carbon Nitride Ohmic Interface for Efficient Photocatalytic Hydrogen Production

*Jun Zhou [a], Junjie Zhang [b], Jing Zhao [a], Haozhi Wang [c], Rui Liu [a]**

[a] Shanghai Key Lab of D&A for Metal Functional Materials, Department of Polymeric Materials, School of Materials Science and Engineering, Tongji University, Shanghai, 201804, China, E-mail: ruiliu@tongji.edu.cn

[b] State Key Laboratory of Materials Processing and Die & Mould Technology, School of Materials Science and Engineering, Huazhong University of Science and Technology, Wuhan 430074, Hubei, China

[c] Key Laboratory of Advanced Ceramics and Machining Technology (Ministry of Education), School of Materials Science and Engineering, Tianjin University, Tianjin 300072, China

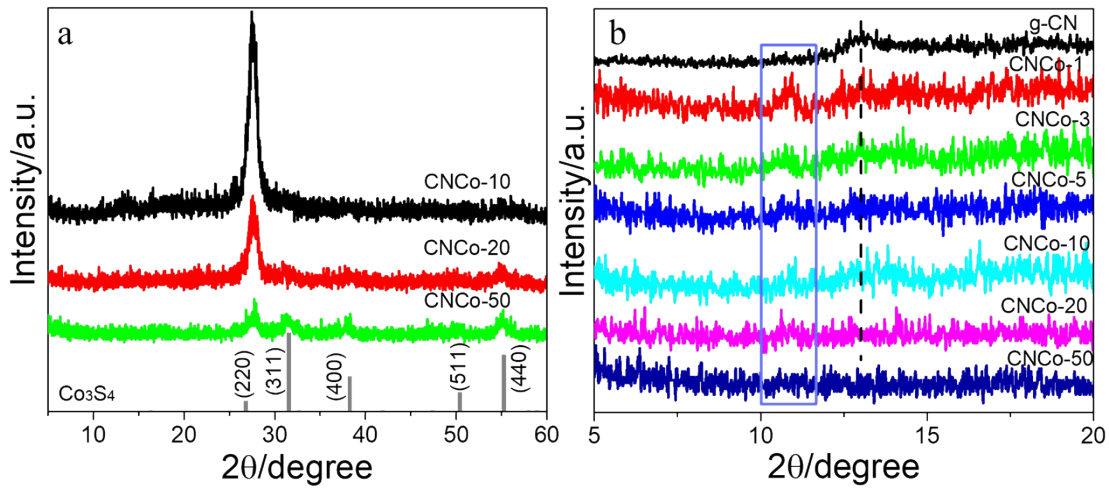

Figure S1 (a) XRD patterns of CNCo-10, -20, -50, (b) XRD patterns of g-CN and CNCo-X in the 2θ range of 5-20°.

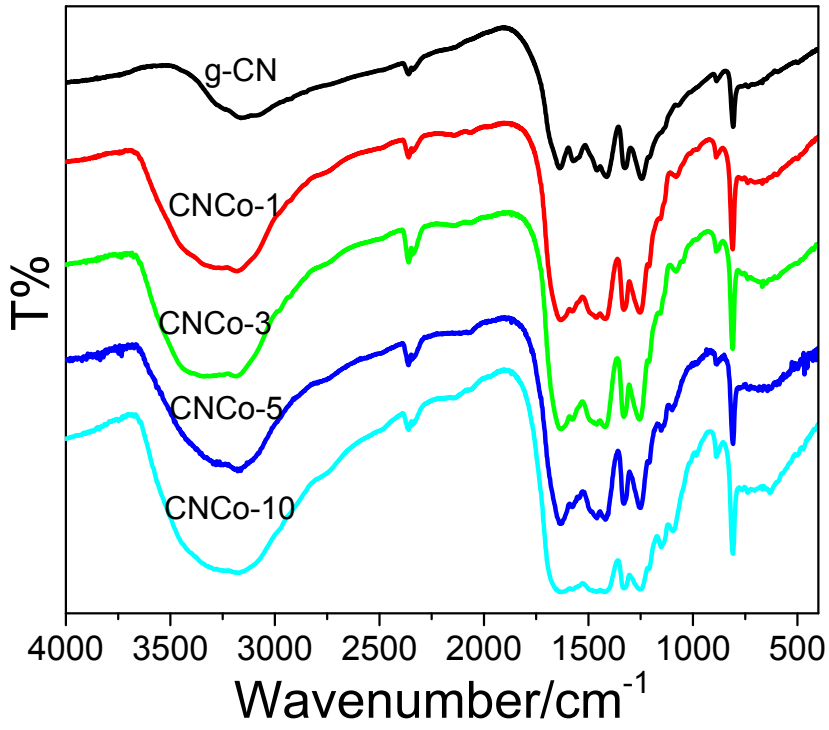

Figure S2 FT-IR spectra of g-CN and CNCo-X.

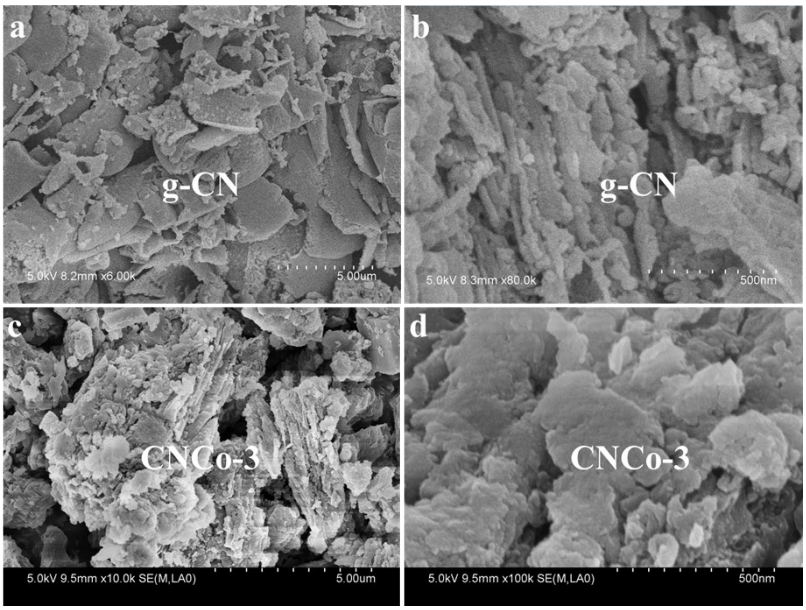

Figure S3 SEM images of g-CN (a-b) and CNCo-3 (c-d).

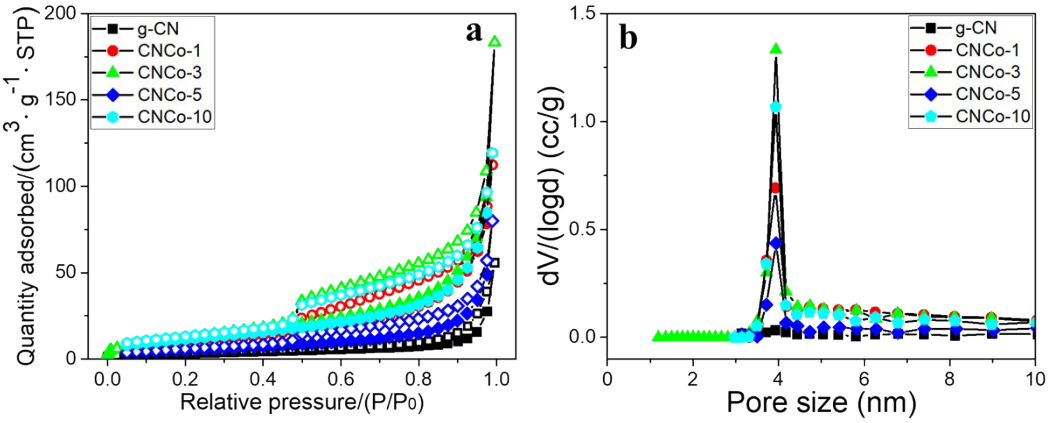

Figure S4 (a) Nitrogen sorption isotherms and (b) pore size distributions for g-CN and CNCo-X samples.

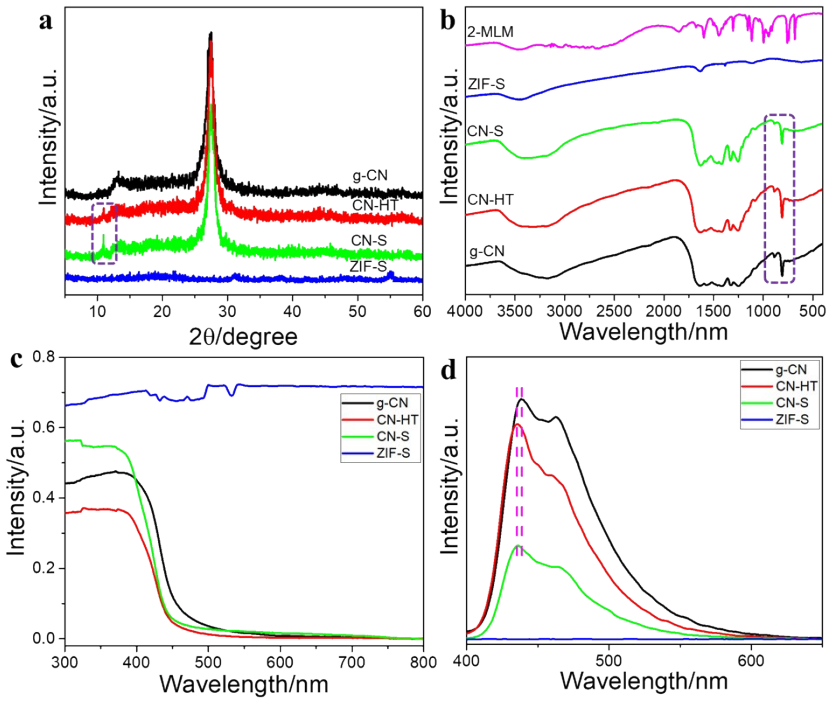

Figure S5 (a) XRD patterns, (b) FT-IR spectra, (c) Ultraviolet-visible diffuse reflectance spectra (UV-Vis DRS), and (d) PL emission spectra of g-CN and the control samples.

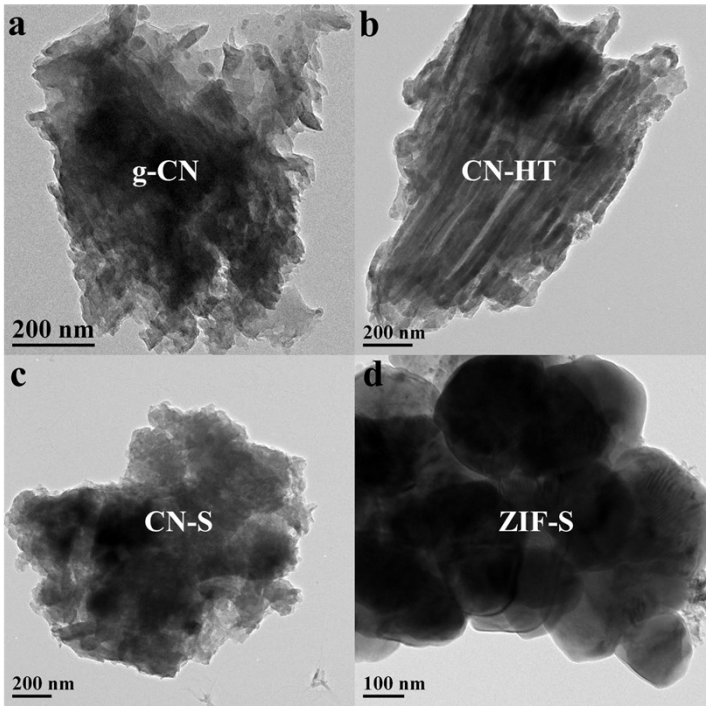

Figure S6 TEM images of (a) g-CN, (b) CN-HT, (c) CN-S, and (d) ZIF-S.

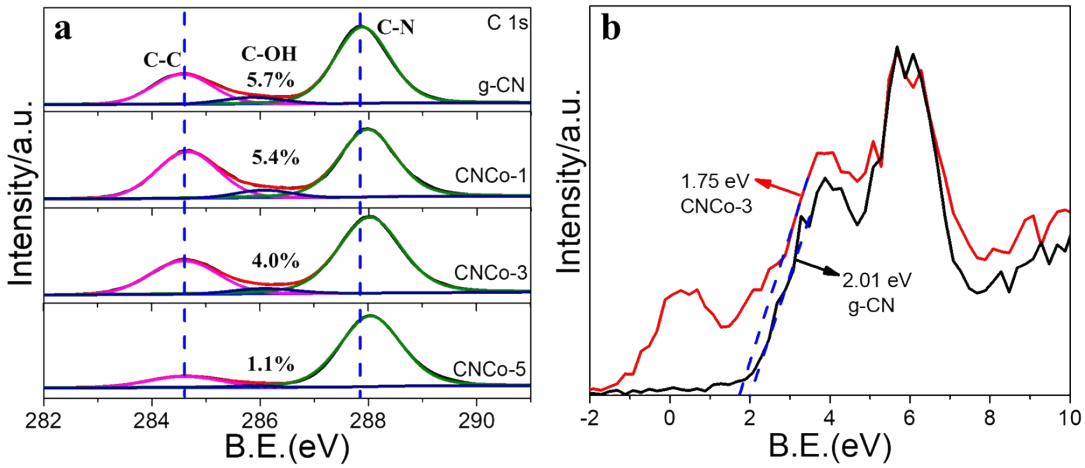

Figure S7 (a) C 1S XPS spectra of g-CN and CNCo-X and (b) Valence band XPS (VBXPS) of g-CN and CNCo-3.

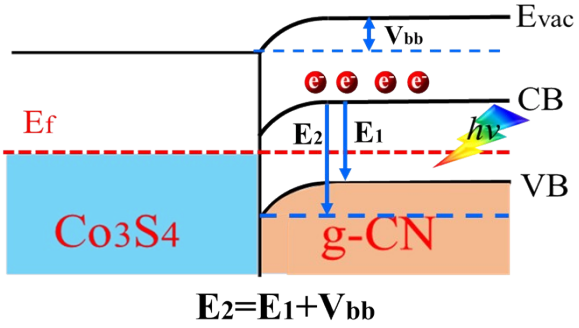

Figure S8 Schematic illustration of PL decay pathway in Co_3S_4-CN junction with downward band bending.

Considering the well-established space charge region formed at metal-semiconductor contact interface, semiconductors are bound to experience band bending induced by built-in eclectic field. When g-CN is excited by photons with energy higher than the band gap, the electrons in the valance band (VB) are promoted into the conduction band (CB). After multiply relaxation process, the electrons will jump back to the ground state mainly by releasing photons (PL emission). In general, the energy of band-edge emission (E_1) is theoretically no larger than the band gap because of the stokes shift. However, owe to the downward band bending in the present case, the energy gap between the VB and CB (E_2) is enhanced. That is, $\mathbf{E_2=E_1+V_{bb}}$, where $\mathbf{V_{bb}}$ is the band bending. As a result, the PL emission will exhibit notable blue-shift as observed in our experiment.

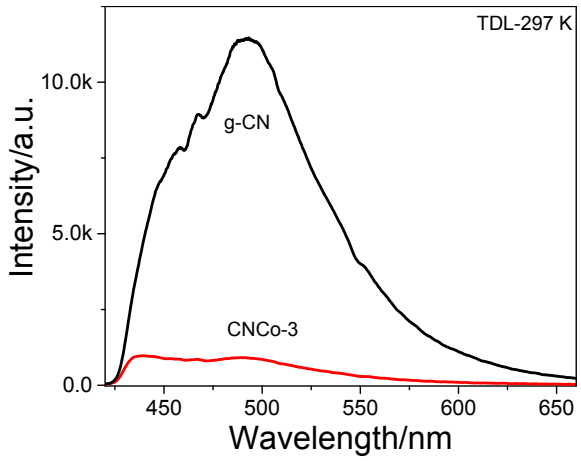

Figure S9 Temperature dependent photo induced luminescence (TDL) at 297 K.

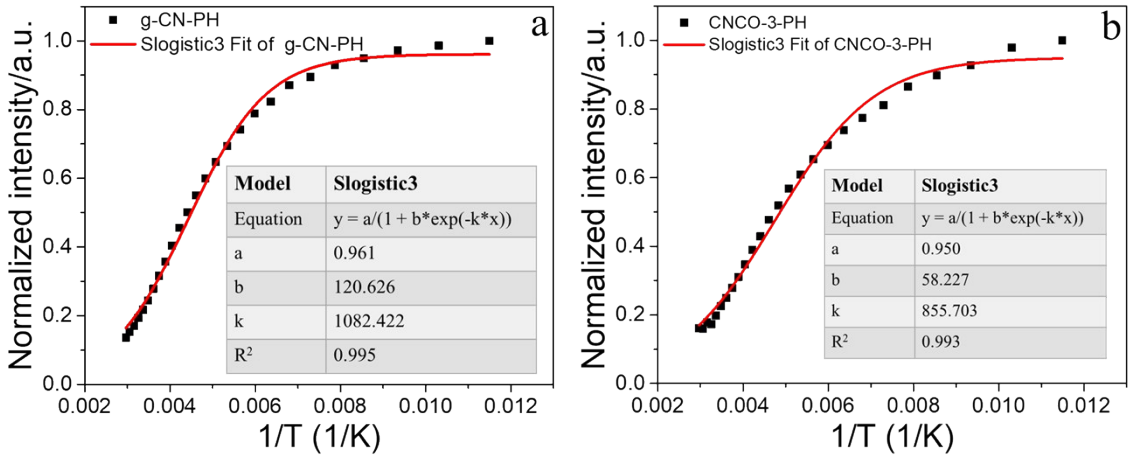

Figure S10 The intensity of PH emission as a function of temperature for (a) g-CN and (b) CNCo-3.

The exciton binding energy E_b is estimated by fitting of temperature dependent PH emission in analogy with that of Arrhenius equation, where k=E_b/K_B and K_B is Boltzmann constant, $8.617*10^{-5}$ eV:

$$I = \frac{I_0}{1 + A\exp(-k/T)}$$

The fitting result and the estimated exciton binding energy are summarized in **Table S2**.

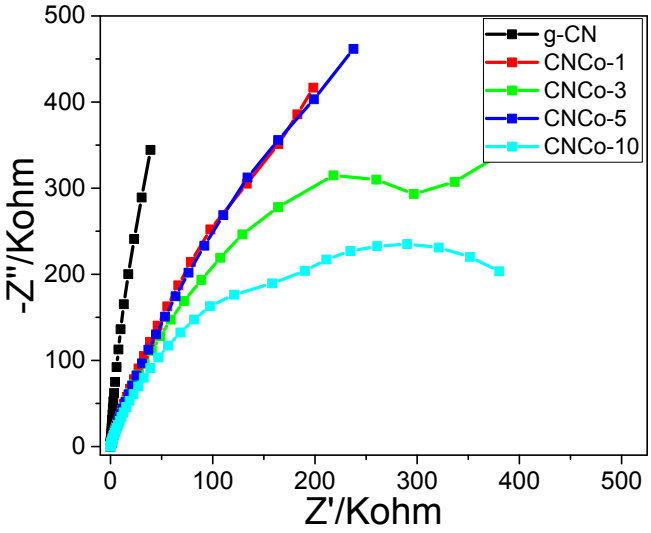

Figure S11 EIS of g-CN and CNCo-X measured on carbon paper supported electrodes without light expose.

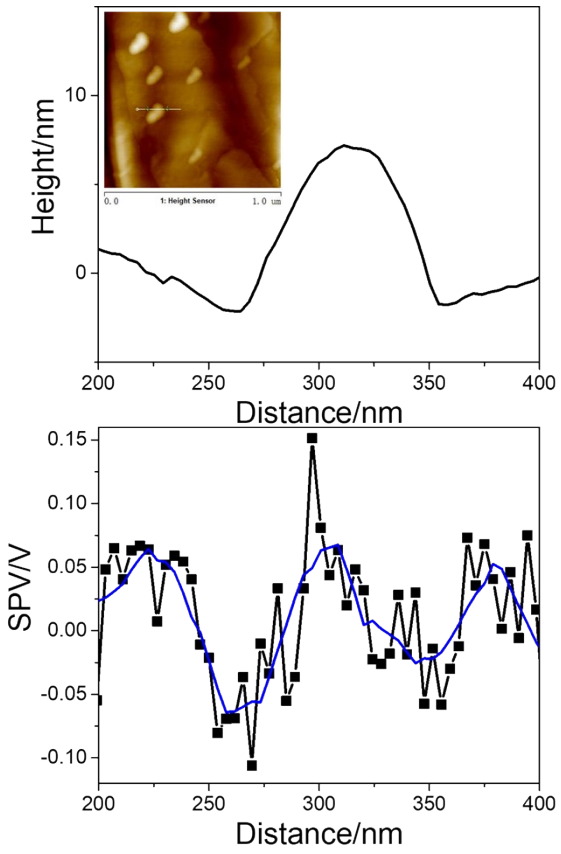

Figure S12 SPV profile of CNCo-3 collected on the particle shown in inset.

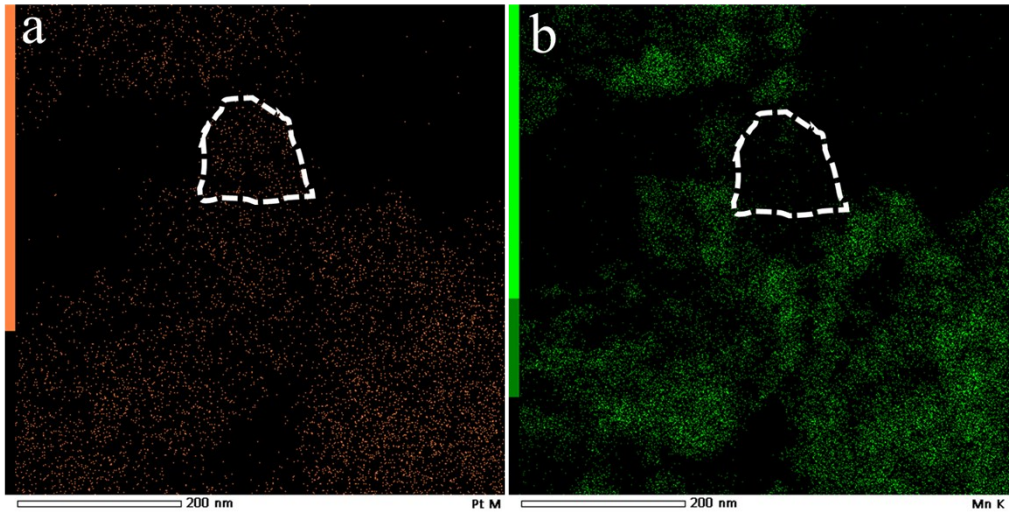

Figure S13 TEM images of the selected area for (a) Pt and (b) Mn element mapping.

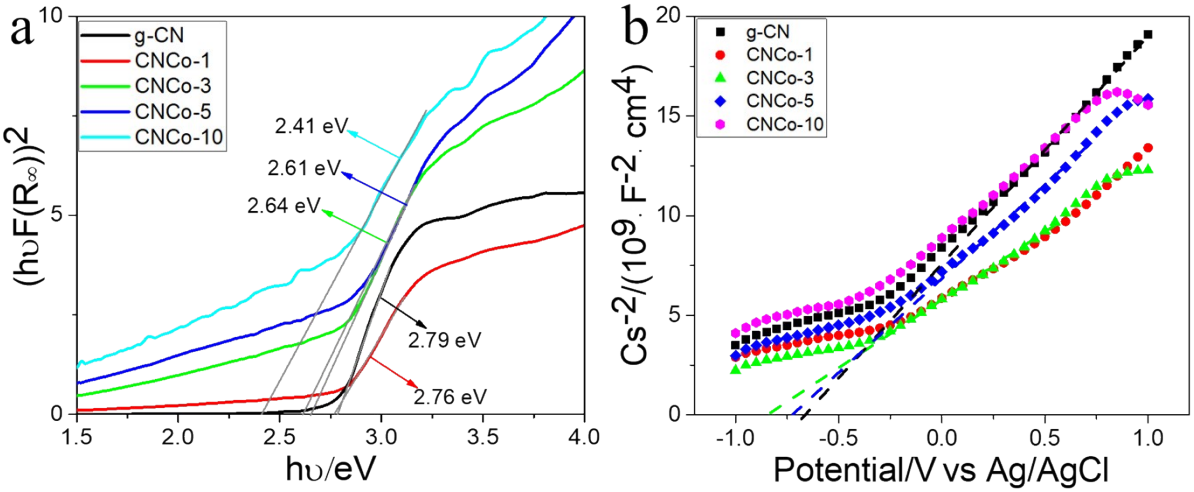

Figure S14 (a) Tauc plot and (b) Mott-Schottky plots of g-CN and CNCo-X.

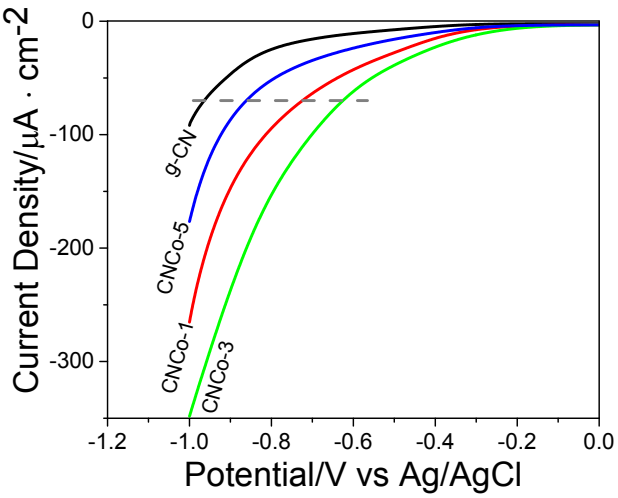

Figure S15 Linear sweep voltammetry (LSV) curves of g-CN and CNCo-X measured in 0.5 M Na_2SO_4 aqueous solution (pH 6.8).

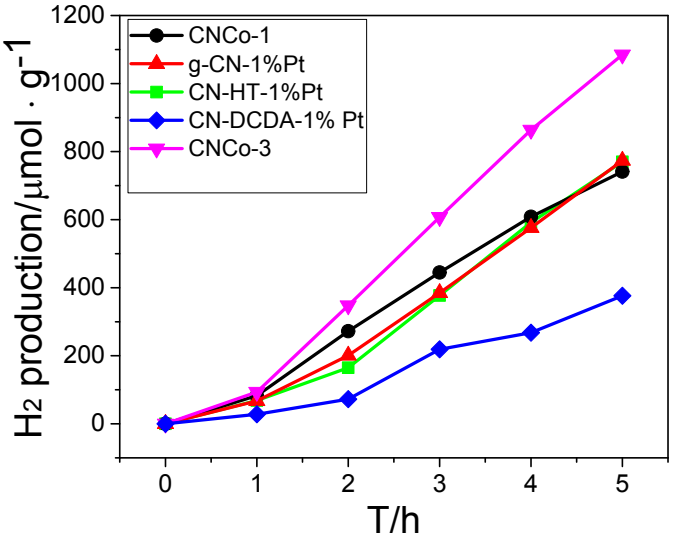

Figure S16 Comparison of photocatalytic activity between Pt loaded control samples (g-CN, CN-HT and CN-DCDA) and CNCo-1/3.

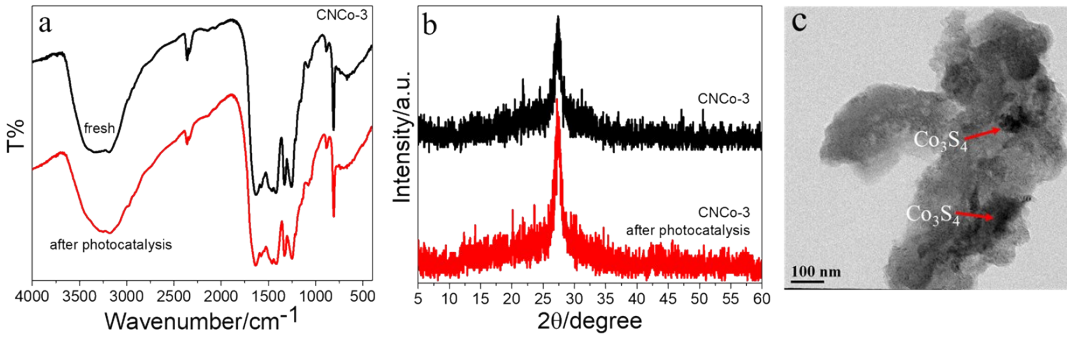

Figure S17 (a) FT-IR, (b) XRD and (c) TEM image of CNCo-3 after photocatalytic hydrogen production.

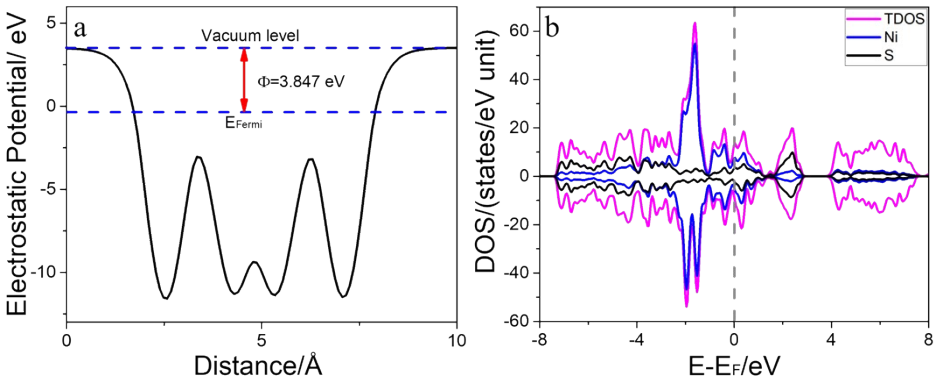

Figure S18 (a) Electrostatic potentials and (b) TDOS of NiS_2 (200) surface.

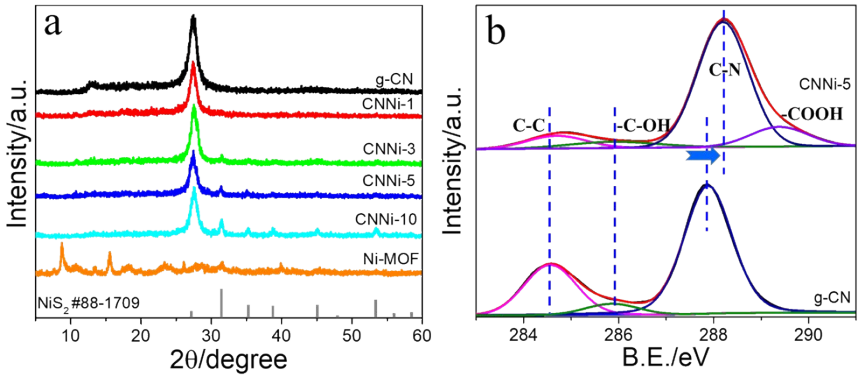

Figure S19 (a) XRD patterns of g-CN, Ni-MOF, and CNNi-X; and (b) XPS C 1S spectra of g-CN and CNNi-5. Note that the unexpected –COOH signal in C 1s spectrum of CNNi-5 was mainly derived from the residual of organic ligand (terephthalic acid: BDC-COOH) of Ni-MOF precursor during hydrothermal reaction.

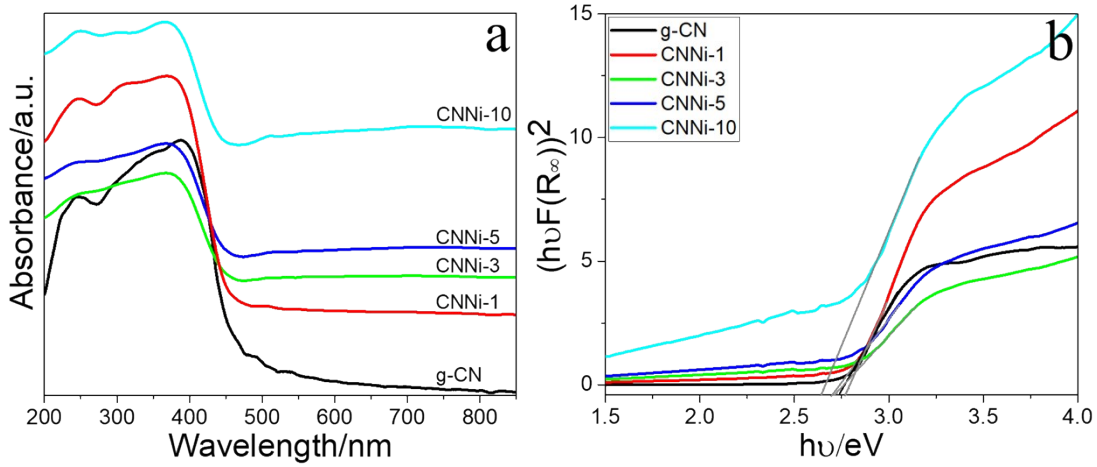

Figure S20 (a) UV-vis absorption and (b) Tauc plot of g-CN and CNNi-X.

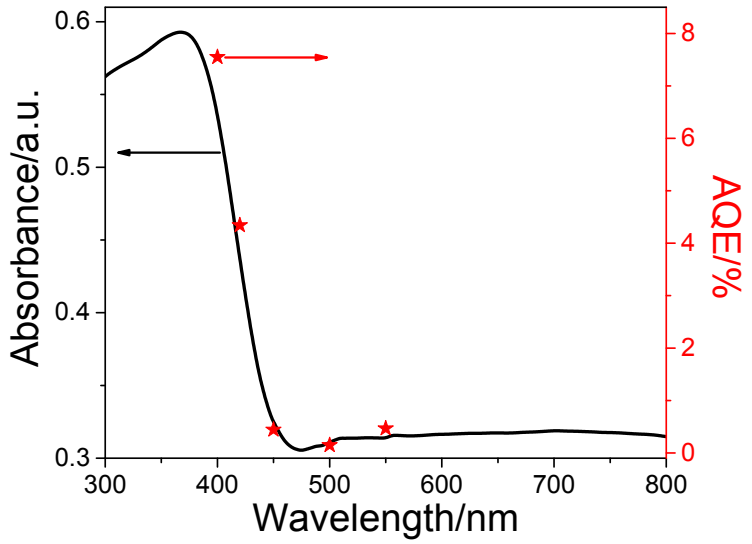

Figure S21 The correlation between the AQE and the light absorption for CNNi-5 measured with band filter of 400, 420, 450, 500, and 550 nm.

Table S1 The fitting results of TRPL decay

.sample	τ_1 (ns)	τ_2 (ns)	τ_3 (ns)	τ_{ave} (ns)
g-CN	4.96 (46.03)	1.26 (46.34)	28.8 (7.63)	14.89
CNCo-1	1.22 (42.09)	4.69 (51.25)	24.93 (6.66)	11.64
CNCo-3	1.29 (45.74)	4.76 (48.23)	25.96 (6.03)	11.76
CNPt-1%	1.22 (51.78)	4.77 (46.46)	27.15 (1.76)	7.30

sample	a	b	k	R^2	E_b/meV
g-CN-PF	0.96	137.33	1083.98	0.994	93.41
g-CN-PH	0.96	120.63	1082.42	0.995	93.27
CNCo-3-PF	0.95	75.44	891.25	0.992	76.80
CNCo-3-PH	0.95	58.23	855.70	0.993	50.18

Table S2 The fitting results of TDL and estimated exciton binding energy.

Table S3 Comparison of H_2 production activity between CNCo-3 and other materials

Photocatalyst	Co-catalyst	Light source	Sacrificial agent	Activity ($\mu mol\ g^{-1}\ h^{-1}$)	Refs
$Co(dcbpy)_2(NCS)_2$/ CQDs/CN	None	Xe lamp (300 W, λ> 420 nm)	TEOA (10 %)	295.9	62
FeP/g-C_3N_4	None	Xe lamp (300 W, λ> 420 nm)	TEOA (10 %)	215	63
In_2O_3/SCN	None	Xe lamp (300 W, λ> 420 nm)	TEOA (10 %)	91.7	64
SWCNT2-PCN	None	Xe lamp (150 W, AM 1.5)	Lactic acid (10%)	29.8	65
MWCNT2-PCN	None	Xe lamp (150 W, AM 1.5)	Lactic acid (10%)	20.5	65
PSCN	None	Xe lamp (500 W, λ> 420 nm)	Methanol (10%)	156.2	66
CNCo-3	None	Xe lamp (300 W, λ> 420 nm)	TEOA (10 %)	217	This work